

# UV-Light Induced Vibrational Coherences, the Key to Understand Kasha Rule Violation in *trans*-Azobenzene

*Artur Nenov<sup>||‡</sup>, Rocio Borrego-Varillas<sup>‡‡</sup>, Aurelio Oriana<sup>†,‡</sup>, Lucia Ganzer<sup>†</sup>, Francesco Segatta<sup>||</sup>, Irene Conti<sup>||</sup>, Javier Segarra-Marti<sup>§</sup>, Junko Omachi<sup>#</sup>, Maurizio Dapor<sup>##</sup>, Simone Taioli<sup>##, +</sup>, Cristian Manzoni<sup>†</sup>, Shaul Mukamel<sup>††</sup>, Giulio Cerullo<sup>†\*</sup>, Marco Garavelli<sup>||\*</sup>*

<sup>||</sup> Dipartimento di Chimica Industriale, Università degli Studi di Bologna, Viale del Risorgimento 4, I-40136 Bologna, Italy

<sup>†</sup> IFN-CNR, Dipartimento di Fisica, Politecnico di Milano, Piazza Leonardo da Vinci 32, I-20133 Milano, Italy

<sup>§</sup> Laboratoire de Chimie UMR 5182, Univ Lyon, ENS de Lyon, CNRS, Université Lyon 1, 46 Allée d'Italie, FR-69342 Lyon, France

<sup>#</sup> Institute for Photon Science and Technology, University of Tokyo, 7-3-1 Hongo, Bunkyo-ku, Tokyo 113-0033, Japan

<sup>‡‡</sup> European Center for Theoretical Studies in Nuclear Physics and Related Areas (ECT\*-FBK) and Trento Institute for Fundamental Physics and Applications (TIFPA-INFN), 38123 Trento, Italy

<sup>+</sup> Faculty of Mathematics and Physics, Charles University, Praha 8, 180 00 Prague, Czech Republic

†† Department of Chemistry, University of California, Irvine, California 92697-2025, US

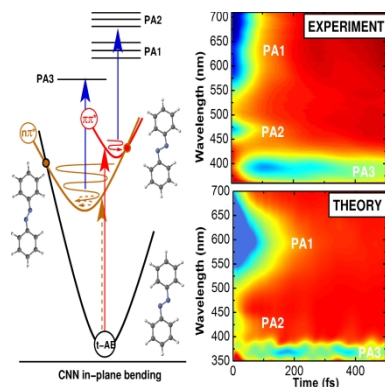
## Corresponding Author

\*marco.garavelli@unibo.it, \*giulio.cerullo@polimi.it

## ABSTRACT

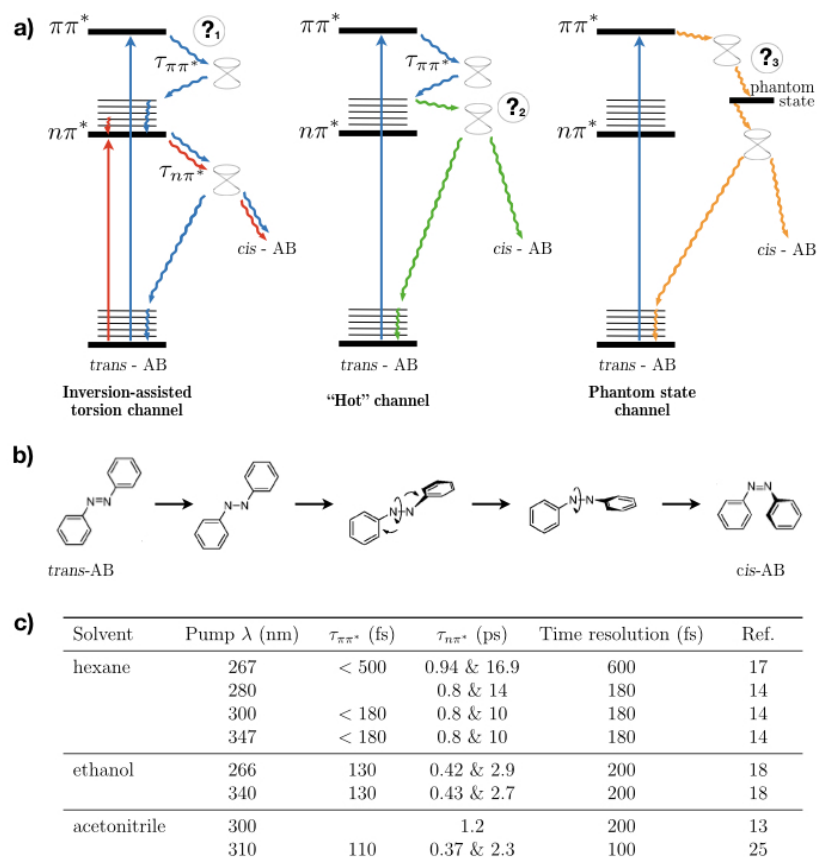
We combine sub-20-fs transient absorption spectroscopy with state-of-the-art computations to study the ultrafast photoinduced dynamics of *trans*-azobenzene (AB). We are able to resolve the lifetime of the  $\pi\pi^*$  state, whose decay within ca. 50 fs is correlated to the build-up of the  $n\pi^*$  population and to the emergence of coherences in the dynamics, to date unobserved. Nonlinear spectroscopy simulations call for the CNN in-plane bendings as the active modes in the sub-ps photoinduced coherent dynamics out of the  $\pi\pi^*$  state. Radiative to kinetic energy transfer into these modes drives the system to a high-energy planar  $n\pi^*/$ ground state conical intersection, inaccessible upon direct excitation of the  $n\pi^*$  state, that triggers an ultrafast (0.45 ps) non-productive decay of the  $n\pi^*$  state and is thus responsible for the observed Kasha rule violation in UV excited *trans*-AB. On the other hand, *cis*-AB is built only after intramolecular vibrational energy redistribution and population of the NN torsional mode.

## TOC GRAPHICS



Photochromism is at the heart of light-powered nanomachines, also known as molecular photoswitches, which can be reversibly switched between two or more stable configurations by exposure to light<sup>1</sup>. Over the years the technological potential of molecular switches has been demonstrated in various applications like optical storage devices<sup>2</sup>, triggers for peptide folding<sup>3-4</sup>, light-gated ion channel control<sup>5</sup> or nonlinear optical materials<sup>6</sup> to name a few. Azobenzene (AB) based compounds are prominent photoswitches which undergo an ultrafast (picosecond) *trans-cis* photoisomerization associated with changing the conformation of the central N=N double bond. AB has favorable photochromic properties, such as a significant change in geometry of the molecule upon isomerization, photoactivity even under strong constraints<sup>7-11</sup> and discrete absorption bands, allowing to selectively address either the *trans* or *cis* configurations. It is therefore not surprising that considerable effort has been put into scrutinizing its photoactivity<sup>8,12-39</sup>. A summary of the most notable research is provided in section 8 of the Supplementary Information (SI). Nowadays it is generally accepted that the decay to the ground state (GS) upon  $\pi\pi^*$  excitation of *trans*-AB involves an extended conical intersection (CI) seam reached through both torsion and bending (“inversion-assisted torsion”, Scheme 1(b)). However, there is still a controversy over key aspects of the photoisomerization process of  $\pi\pi^*$ -excited *trans*-AB. To date the temporal resolution of transient experiments has not permitted to determine the lifetime of the  $\pi\pi^*$  state

(?<sub>1</sub> in Scheme 1(a)). To the best of our knowledge a value of 110 fs<sup>25</sup> is the shortest lifetime reported in the literature, which is comparable to the used instrumental response function (see Scheme 1(c)) for a literature survey of  $\pi\pi^*$  and  $n\pi^*$  lifetimes after  $\pi\pi^*$  excitation). Following the ultrafast decay of the spectral features associated with the  $\pi\pi^*$  state a bi-exponential (sub-ps and several ps) decay of the  $n\pi^*$ -associated signatures has been reported. While there is strong evidence for a pathway common to  $\pi\pi^*$ - and  $n\pi^*$ -excitation<sup>18,20,25-26</sup> (i.e. inversion-assisted torsion, shown in blue and red in Scheme 1(a)) it is still unclear what is the nature of the molecular motion associated with the sub-ps relaxation dynamics. It is speculated that this ultrafast channel involves a CI inaccessible upon  $n\pi^*$  excitation<sup>25,29</sup> (labeled “hot” channel in Scheme 1a)), but it is yet to be demonstrated whether this relaxation channel is reactive (i.e. leading to *cis*-AB) or non-reactive and whether it is responsible for the violation of Kasha rule<sup>8</sup>, characterized by a 50% decrease of the quantum yield (QY) upon excitation of *trans*-AB with UV light (?<sub>2</sub> in Scheme 1a)). Related to this, the involvement of “dark” states (labeled “phantom” state in Scheme 1a)), brought into discussion by several authors<sup>21,28,33</sup> as a possible reason for the QY decrease, still remains controversial (?<sub>3</sub> in Scheme 1a)).



**Scheme 1.** a) Energy diagrams of the relaxation channels in *trans*-AB after  $n\pi^*$ - and  $\pi\pi^*$ - excitation, proposed in the literature. b) The *trans*→*cis* mechanism of inversion-assisted torsion. c) A literature survey of the of  $\pi\pi^*$  and  $n\pi^*$  lifetimes after  $\pi\pi^*$  excitation.

In this paper, we address these questions by combining high time resolution transient absorption (TA) spectroscopy and multiconfigurational wavefunction techniques. We perform TA with sub-20-fs pump pulses at 320 nm and broadband probe pulses ranging from the visible (350-700 nm) to the UV (250-380 nm), which: (a) allow to resolve the dynamics in the  $\pi\pi^*$  state prior to its ultrafast (sub-100 fs) decay; (b) resolve coherent ES dynamics in the  $n\pi^*$  state; (c) explore the deep UV window (250-280 nm) rich with spectroscopic fingerprints of reactant and photoproduct. *Ab initio* molecular dynamics (MD) simulations within the second order multi-configurational perturbation theory (CASPT2)

framework utilizing a full- $\pi$  active space disclose the relaxation routes from the Franck-Condon (FC) point on the  $\pi\pi^*$  state to the GS, thereby confirming the ultrafast  $\pi\pi^* \rightarrow n\pi^*$  decay. The simulations show that the “hot”  $n\pi^*$  population can decay to the GS through an energetically high lying near-planar region of the  $n\pi^*/GS$  CI seam not accessible upon selective excitation of the  $n\pi^*$  state, thus confirming the existence of the “hot” decay channel (Figure 1a)). We argue that this channel is non-reactive and, thus, the prime reason for the violation of the Kasha rule. Combining high-level electronic structure calculations with theoretical nonlinear spectroscopy techniques we simulate the TA spectra, explicitly incorporating the, so far, theoretically elusive excited state absorption (ESA) features and their vibrational lineshape broadening, therefore uncovering the nature of the coherent oscillations observed in the experiment.

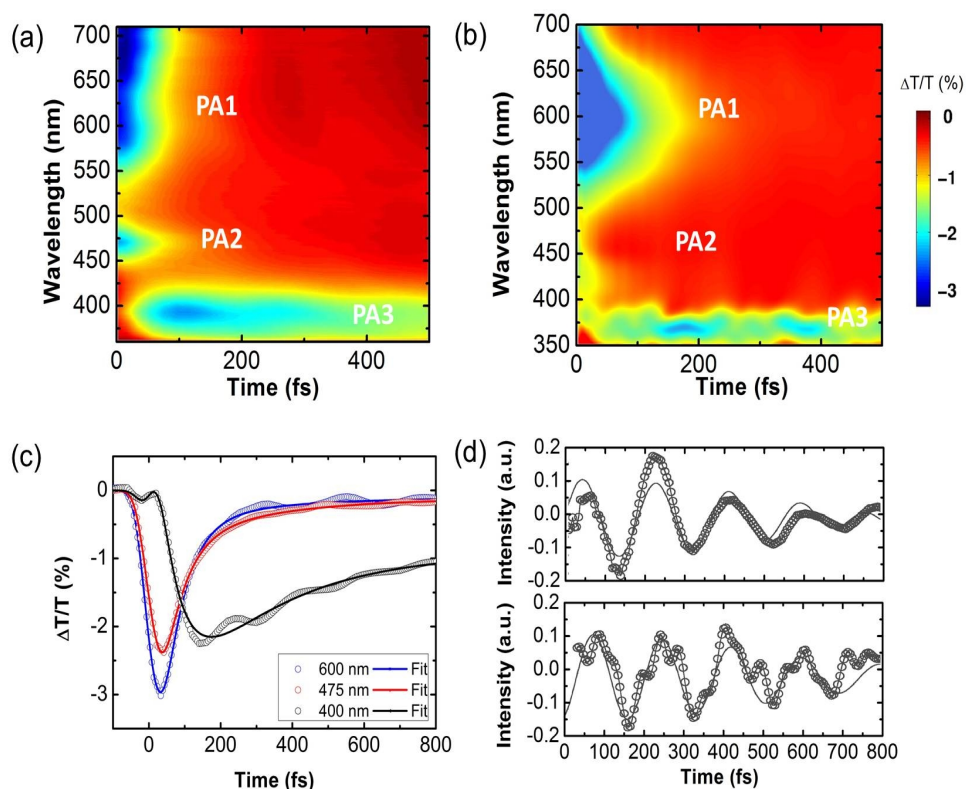


**Figure 1.** (a) Experimental (ethanol) and (b) theoretical (gas-phase) TA maps of *trans*-AB in the visible spectral window during the first 500 fs with (c) extracted dynamics at 400, 475 and 600 nm. (d) Intensity oscillations (residuals): experimental at 400 nm (top) and computed at 370 nm (bottom). Open dots represent the experimental (theoretical) data and the solid line the fits.

*Trans*-AB in ethanol solution was pumped with 16-fs UV pulses centered at 330 nm, resonant with the  $\pi\pi^*$  transition, and probed over a broad wavelength range. The experimental setup has been described elsewhere<sup>40-42</sup>, whereas the sample preparation details and the linear absorption (LA) spectrum are provided in the SI. Figure 1(a) shows the TA spectra in the visible (VIS) between 360-700 nm for the first 500 fs. In agreement with previous studies<sup>14,17,18,25</sup>, at early times (<100 fs) we observe two photoinduced absorption (PA) bands: a broad intense band ranging from 550 nm to 700 nm (PA1) and a narrower band between 450 nm and 500 nm (PA2). A global fit of the data<sup>49-50</sup>(see SI for details) reveals that PA1 and PA2 decay with a lifetime of  $\sim 50$  fs (Figure 1(c)), with the concurrent rising of a new PA band (PA3), formed with the same time constant, peaking around 400 nm. Considering their ultrafast decay and their absence in the spectra when the  $n\pi^*$  state is selectively excited, PA1 and PA2 have been previously assigned to the  $\pi\pi^*$  state<sup>18,25-26</sup>. PA3, on the other hand, is a fingerprint of the  $n\pi^*$  state<sup>18-20,25,26</sup>. It shows oscillatory behavior with a period of 170 fs ( $195\text{ cm}^{-1}$ ), an indication of coherent dynamics, damped after  $\approx 2$  ps. Similar oscillatory patterns are observed also at 600 nm and 670 nm, after the initial fast amplitude decay. Measurements on longer timescale (Figures S20 and S21, SI) show a PA3 decay described by the sum of three exponentials with time constants 0.45ps, 2.5 ps and  $\sim 9$  ps, in agreement with previous studies<sup>18-20,25</sup>.

Figure 1(b) depicts the simulated TA map in the same temporal and spectral windows. The simulations protocol utilizes non-linear response theory, the system's response to the perturbation by

three external electric fields is expressed within the framework of cumulant expansion of Gaussian fluctuations (CGF)<sup>43-45</sup> and the parameters were obtained with electronic structure computations within the framework of multi-configurational wavefunction theory<sup>46-48</sup>. The simulation protocol is outlined in Sections 1 and 2 of the SI. Despite the notable blue-shift of the computed signals with respect to experiment (that falls within the accuracy of the computational approach) the agreement is excellent. These results allow us to identify the nature of the underlying transitions. The rapidly decaying PA1 and PA2 features are fingerprints of the  $\pi\pi^*$  state, which arise due to the spectral overlap of ESA bands associated with several electronic transitions. Each of the two ESA signals consists of three higher lying states which are bright from the  $\pi\pi^*$  state and have a pronounced multiconfigurational nature and significant weights of doubly excited configuration state functions (SI, PA1: section 3.2.2, Figure S12 and Table S5).

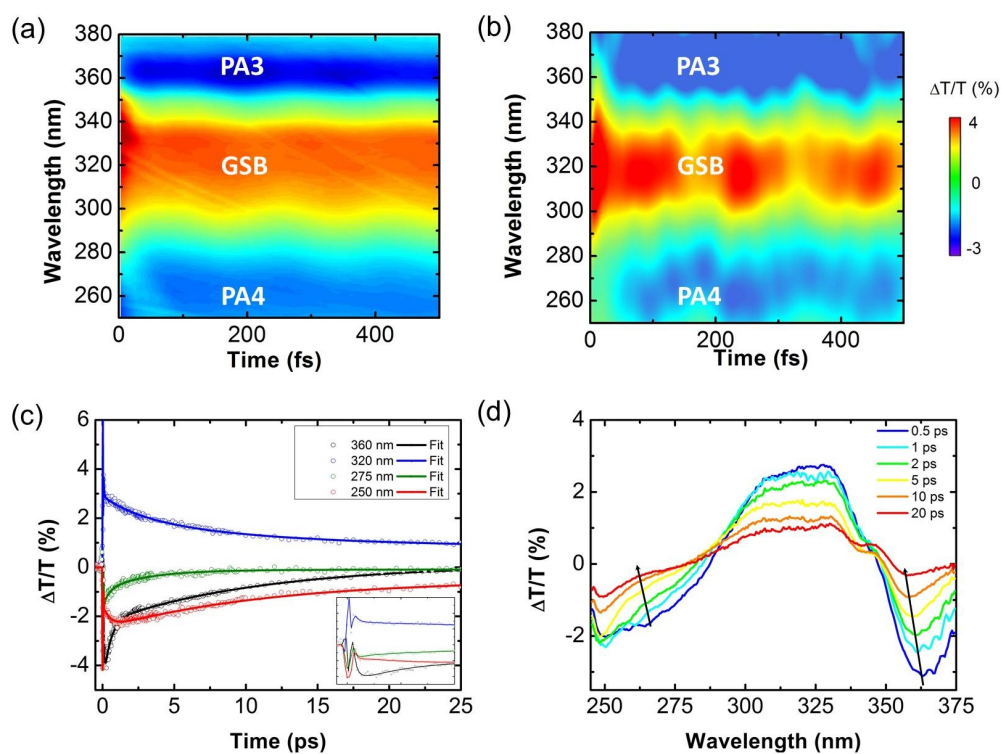


**Figure 2.** (a) Experimental (ethanol) and (b) theoretical (gas-phase) TA data of *trans*-AB probed in the ultraviolet range (245-380 nm). (c) Extracted dynamics at three selected wavelengths (open circles) and fit of the data (solid lines). Inset: Zoom up to 2 ps delay time. (d) Extracted transient spectra at several delay times. Arrows highlight the blue-shift of the maxima of the transient absorption signals around 270 nm and 360 nm.

ESA bands provide an indirect probe of the coherent vibrational dynamics in the ES reflected in peak shifts and intensity beats, whose magnitude is correlated to the electronic structure of the underlying states. The states contributing to PA1 and PA2 show pronounced sensitivity to following ES-active modes: 606/614  $\text{cm}^{-1}$ , 666  $\text{cm}^{-1}$ , 924  $\text{cm}^{-1}$ , 1161  $\text{cm}^{-1}$ , 1397  $\text{cm}^{-1}$  and 1628  $\text{cm}^{-1}$ , associated with bending and stretching deformations in the central CNNC fragment (Figures S5 and S6 in the SI). The ultrafast decay of the population covers coherent oscillatory features at early times. The picture is clearer when looking at the 400 nm trace (Figure 1(c)), the fingerprint of the  $n\pi^*$  state. It arises from a single ESA contribution to a higher lying state (SI, section 3.2.3 and Table S6). As noted above, the intensity of PA3 shows clear oscillatory behavior with a 170-fs period. Our simulations (Figure 1(d)) reproduce the intensity beat pattern rather well. Remarkably, only one dominant vibrational feature (195  $\text{cm}^{-1}$ ) is extracted from both the experiment and simulation despite the fact that time-resolved Raman<sup>17</sup> and photoionization<sup>31</sup> spectroscopies have resolved a plethora of modes involved in the coherent dynamics on the  $n\pi^*$  state after selective  $n\pi^*$  excitation. Oddly enough, although the CASSCF frequencies at the  $n\pi^*$  minimum provide a 205  $\text{cm}^{-1}$  mode (symmetric CNN bending) that could be tentatively assigned to the experimental observation, our simulations demonstrate that the ES responsible for PA3 is rather insensitive to the dynamics in this mode (Figure S8, SI). Instead, our simulations show that the 660  $\text{cm}^{-1}$  and 852  $\text{cm}^{-1}$  modes, both having strong CNN bending contribution,

strongly modulate the absorption cross-section of the ES and are the source of the observed intensity beats (see Chapter 3.2 in the SI). These frequencies have been reported to be particularly intense in time-resolved Raman studies<sup>15, 25</sup> and in photoionization spectroscopy<sup>31</sup>. Together with the 205 cm<sup>-1</sup> CNN bending and the 300 cm<sup>-1</sup> CCN bending modes, they constitute a quartet of “hot” modes that accumulate almost 10000 cm<sup>-1</sup> reorganization energy upon  $\pi\pi^* \rightarrow n\pi^*$  decay. We also note a second  $n\pi^*$  fingerprint PA signal around 600 nm which has been reported previously for selective  $n\pi^*$  excitation<sup>18,25</sup>. Weak coherent oscillations are resolved in the ps-range. For this ESA three modes, 205 cm<sup>-1</sup>, 660 cm<sup>-1</sup> and 852 cm<sup>-1</sup> are predicted to contribute (Figure S13 in the SI).

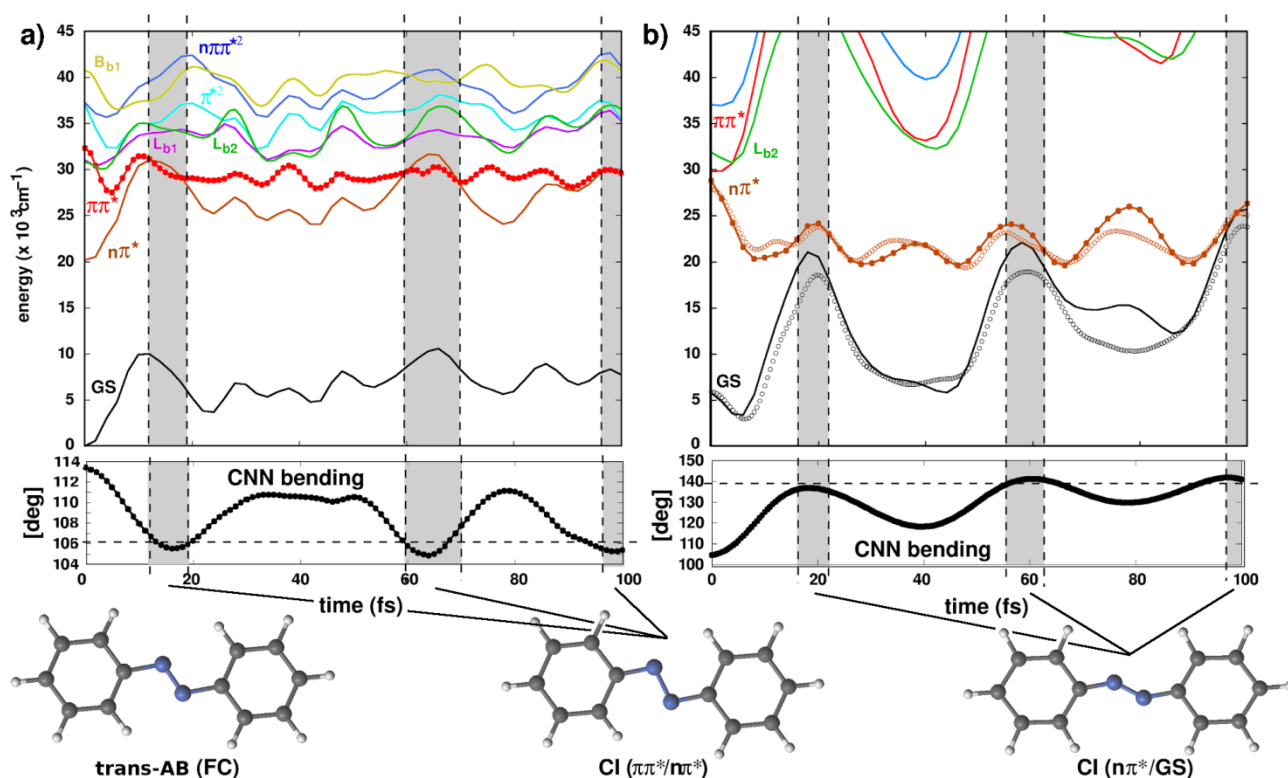


**Figure 3.** Structure of the low-lying ES manifold along the 0K MD in the  $\pi\pi^*$  state (red) initiated at the FC point (a) and along the  $n\pi^*$  state (brown) initiated at a CI between  $\pi\pi^*$  and  $n\pi^*$  (b). Both, symmetry-constrained (solid lines) and fully unconstrained (dashed lines) simulations were performed starting from a planar and a non-planar CI geometry, respectively. The evolution of CNN bending along the

symmetry-constrained trajectories is shown. Gray areas indicate recurrent crossings between  $\pi\pi^*$  and  $n\pi^*$  (a), as well as between  $n\pi^*$  and GS.

A second set of measurements was performed with UV (250-380 nm) probe. Figure 2(a) shows the TA map during the first 500 fs compared to the theory (panel (b)). A longer timescale measurement is given in the SI (Figures S20 and S21). In addition to PA3, two new spectral features are observed: the GSB in the range 300-340 nm, which decays with a time constant of 11 ps (Figure 2(c)) and a PA band ranging from 245 to 280 nm (PA4). Global analysis reveals 0.46, 2.8 and 11 ps time constants. These values match those of PA3, indicating that the nature of PA4 and PA3 must be similar. This notion is supported by the computations, which resolve also this ESA feature of the  $n\pi^*$  state (Figure 2(b) and SI, section 2.2.3 and Table S6). There is, however, one noticeable difference between PA3 and PA4: by comparing the TA spectra (Figure 2(d)), one observes that while the signals at 365 nm and 270 nm decrease in amplitude during the first 2 ps accompanied by a blue-shift, PA4 shows a simultaneous increase in amplitude at the bluest frequencies (245-260 nm) on the same timescale. At longer delay times the entire band relaxes with a lifetime of 11 ps, leaving a finite long-lived offset due to the formed *cis*-AB. Correspondingly, a fit of the signal at 250 nm shows a build-up time of 0.46 ps, and decay constant of 11 ps. A global analysis of the data (SI, Figure S23) reveals that the bluest region (245-260 nm) is dominated by the 0.46 ps and 11 ps components, whereas in the reddest region (260-280 nm) the 0.46 and 2.8 ps components present the largest amplitude. Thus, these two spectral regions of PA4 capture different processes whose signatures overlap spectrally and temporally. The LA spectrum of *cis*-AB (see Figure 1 in ref. 25) shows a peak at 250 nm. Thus, one might tentatively assign the build-up of intensity at this wavelength to the formation of *cis*-AB in the GS on a sub-ps time scale. However, we argue that we observe more probably a signature of the “hot” *trans*-AB reactant. Kovalenko *et al.*

estimated that  $\approx 50\%$  of the  $n\pi^*$  population returns to the GS within the first ps. Even if we assumed that all of the *cis*-AB photoproduct ( $\sim 12\%$  QY) is formed through this ultrafast channel, at least four times more “hot” reactant would be recovered simultaneously. It is well known that a “hot” GS gives rise to a PA band red-shifted from the GSB, which decays by vibrational cooling on a ps time scale. The LA spectrum of *trans*-AB has a narrow band peaking at  $\approx 230$  nm, assigned by our computations to a transfer of electronic density between the central CNNC fragment and the benzene rings (SI, Table 4). Thus, we interpret the 250-nm signal as the build-up of the “hot” GS of the reactant, whose PA overlaps with the 270 nm ESA of the  $n\pi^*$  state.

To validate this interpretation and explain the molecular motions governing the ultrafast (sub-ps) decay of a major part of the ES population, we performed adiabatic *ab initio* MD simulations utilizing quantum mechanical gradients at CASPT2 level of theory<sup>51</sup> (Figure 3). A single trajectory was initiated in the FC point ( $C_{2h}$  symmetry) of the bright  $\pi\pi^*$  state (red dotted line in Figure 3(a)) without initial kinetic energy and the energies of the close lying electronic states were monitored for the first 100 fs (further details on the simulation protocol are provided in Chapter 4 of the SI). We found a high density of electronic states in the near- and deep-UV energy window (250-400 nm). Two spectroscopically “dark” states involving the benzene rings (purple, Lb1, and green, Lb2, SI, Table S4) appear near isoenergetic with the  $\pi\pi^*$  state in the FC point. Further states involve the doubly excited  $\pi^{*2}$  (cyan), the mixed  $n\pi\pi^{*2}$  transition (blue) and the aforementioned “bright” state responsible for the 230 nm band in the LA spectrum (Bb1, shown in dark ocher, SI, Table 4). The picture is completed by the  $n\pi^*$  state at  $\sim 500$  nm, the lowest ES in *trans*-AB. In agreement with Raman data<sup>15,23,31</sup> the vibrational dynamics in the  $\pi\pi^*$  state is governed by the N=N and C-N stretching modes with  $1397\text{ cm}^{-1}$  and  $1618\text{ cm}^{-1}$  frequencies. It is apparent that the  $\pi\pi^*$  state crosses several times with the  $n\pi^*$  state, which exhibits a

pronounced destabilization in intervals of ca. 40 fs. These recurrent crossings (gray areas in Figure 3(a)) are correlated to the in-plane CNN bending. We clarify, however, that the  $\pi\pi^* \rightarrow n\pi^*$  population transfer is symmetry-forbidden for planar geometries. Out-of-plane deformations are required to invoke a non-zero non-adiabatic coupling. Upon releasing the symmetry constraints we optimized a non-planar asymmetric CI (SI, Chapter 2.2.3) with a CNNC dihedral of  $13^\circ$ . It is, thus, evident that an extended non-planar  $\pi\pi^*/n\pi^*$  CI seam is available to *trans*-AB. The need to undergo out-of-plane deformations for efficient population transfer might explain the mismatch between the experimental  $\pi\pi^*$  lifetime of 52 fs and the theoretical simulation revealing a crossing as early as 15 fs.

The “dark” benzenic<sup>17</sup> and the doubly excited  $\pi\pi^{*2}$  states have been suggested to participate in the deactivation of the  $\pi\pi^*$  state<sup>28,33</sup> (“phantom” states). The best candidate for a potential population bifurcation is one of the benzenic states Lb2 (green line in Figure 3(a)) due to its energetic proximity to the  $\pi\pi^*$  state and to the finite (symmetry-allowed) probability for non-adiabatic population transfer even for planar geometries. However, our simulations show that this state remains above the  $\pi\pi^*$  state throughout the dynamics, suggesting that the direct  $\pi\pi^* \rightarrow n\pi^*$  decay is the most efficient channel, in agreement with our high time resolution TA results. We emphasize that the OK simulations do not disprove the participation of “phantom” states but merely show that latter are not necessary to rationalize the spectroscopic features of the present study.

Starting from the non-planar CI geometry we followed the molecular dynamics in the  $n\pi^*$  state through a fully unconstrained simulation for 200 fs (dashed lines in Figure 3(b)). We chose the non-planar geometry as a starting point of the simulation to address potential activation of either the (asymmetric) inversion or the torsion mechanism at early times. MD simulations were also performed under  $C_{2h}$  symmetry (solid lines in Figure 3(b)) starting from a planar  $\pi\pi^*/n\pi^*$  CI. The  $n\pi^*$  exhibits a

pronounced destabilization in the  $\pi\pi^*/n\pi^*$  CI region, due to the far out-of-equilibrium displacement along the CNN coordinate with a value of  $127^\circ$  in the  $n\pi^*$  equilibrium. After crossing to the  $n\pi^*$  state the wavepacket converts upon relaxation nearly  $10000\text{ cm}^{-1}$  potential energy, stored in the CNN bending modes, to kinetic energy. Despite the unconstrained approach, we observe only in-plane dynamics during the first 200 fs governed by the same four “hot” CNN modes responsible for the intensity beat pattern observed in the VIS spectra. In fact, the unconstrained dynamics follows closely the dynamics within  $C_{2h}$  symmetry. The vibrational energy inserted in the bending modes drives AB within 20 fs away from the  $\pi\pi^*/n\pi^*$  CI far beyond the  $n\pi^*$  equilibrium towards a CI with the GS situated  $\sim 5000\text{ cm}^{-1}$  above the  $n\pi^*$  minimum and showing an increase of the CNN angles to  $143^\circ$ <sup>29</sup>. The CI region is revisited every 40 fs. It is this energetically high lying segment of the CI seam with nearly planar geometries, which remains inaccessible after direct  $n\pi^*$  excitation, that effectively funnels half of the  $n\pi^*$  population back to the GS within the first 500 fs after  $\pi\pi^*$  excitation. We argue that this channel should be essentially non-reactive because: a) we do not observe the activation of asymmetric bending modes required to reach *cis*-AB; b) a finite barrier exists in the GS along the  $143^\circ \rightarrow 180^\circ$  CNN increase required to reach the transition state region; c) the crossing seam is a turning point in the dynamics along the CNN coordinate. This would account for the drop in photoisomerization efficiency when exciting  $\pi\pi^*$  as compared to  $n\pi^*$  excitation. Finally, 1.5-ps long MD simulations (performed for technical reasons at CASSCF level) reveal that intramolecular vibrational redistribution (IVR) from the bending and stretching modes into the torsional mode occurs on a 1-ps time scale (SI, Figure S17). Thus, we associate the experimental 2.8-ps lifetime to the decay of the remaining  $n\pi^*$  population through the widely accepted torsional mechanism.

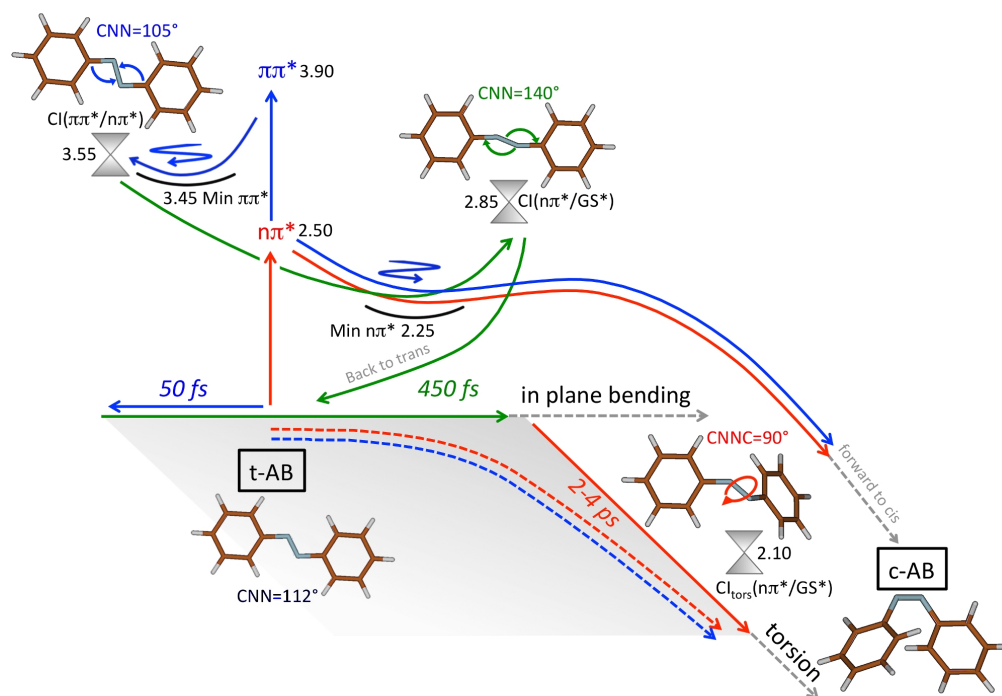


**Figure 4.** Overview of the photochemistry of *trans*-AB in the space of the CNN in-plane bending and CNNC torsion modes. Excitation of the bright  $\pi\pi^*$  transition in the UV (320 nm) opens a sub-ps non-reactive decay channel to the GS via  $\pi\pi^* \rightarrow CI(\pi\pi^*/n\pi^*) \rightarrow n\pi^* \rightarrow CI(n\pi^*/GS)$  (“hot” channel in Scheme 1a)). The coherent dynamics associated with this non-reactive channel driven by the in-plane CNN bending mode is the source of ESA intensity beats in the transient spectra and reduced QY. *trans*  $\rightarrow$  *cis* isomerization requires IVR into the torsional mode, takes an order of magnitude longer (2-4 ps), is incoherent and proceeds in analogous way upon UV and VIS excitation (500 nm,  $n\pi^*$  excitation). Dashed lines show projection in the bending-torsion plane. Coloring according to Scheme 1a). Energy values in eV.

In conclusion, we have combined TA spectroscopy with sub-20 fs temporal resolution in the UV range with state-of-the-art computational tools to study the ultrafast photodynamics of *trans*-AB. We

were able to resolve the lifetime of the  $\pi\pi^*$  state, the build-up of the  $n\pi^*$  population and the following coherent oscillatory dynamics. We observe a single ultrafast lifetime ( $\sim 50$  fs) of the  $\pi\pi^*$  state which is correlated to the build-up of the  $n\pi^*$  ESA. Theoretical simulations reproduce with remarkable accuracy the positions of all ESA bands from the  $\pi\pi^*$  and  $n\pi^*$  states and reveal the origin of the ps-lasting oscillations of the intensity of the photoinduced absorption signals and, thus, the nature of the vibrational dynamics activated immediately after decay to the  $n\pi^*$  state. Four “hot” modes, all characterized by strong symmetric in-plane bending deformations in the central CNNC fragment, were identified:  $200\text{ cm}^{-1}$ ,  $300\text{ cm}^{-1}$ ,  $650\text{ cm}^{-1}$ ,  $850\text{ cm}^{-1}$ . The observed intensity beat pattern is a signature of the localization of large amount of energy ( $10000\text{ cm}^{-1}$ ) in these four modes during the first 1 ps causing strong modulations of the absorption cross section. Radiative to kinetic energy transfer opens a non-radiative channel to the GS, inaccessible upon  $n\pi^*$  excitation (Figure 4). The interplay between theory and experiment allows us to assign the so-called “CNN-bending” channel as the main reason behind the violation of the Kasha rule and behind the QY reduction at shorter wavelengths, *cis*-AB being formed only after IVR from the bending modes into the torsion on the ps time scale. Finally, neither the experimental nor the theoretical results call for additional ESs in order to describe the  $\pi\pi^*$  depopulation dynamics: all experimental spectral features can be accurately reproduced using only the  $\pi\pi^*$  and  $n\pi^*$  states.

## ASSOCIATED CONTENT

**Supporting Information.** Sample preparation, LA spectrum, experimental setup, results of the data analysis, simulation protocols for non-linear spectroscopy and molecular dynamics, simulation parameters, simulated spectra, molecular orbitals and Cartesian coordinates.

The following files are available free of charge.

## AUTHOR INFORMATION

### Notes

‡These authors contributed equally.

⊥Present address: École Polytechnique Fédérale de Lausanne, CH-1015 Lausanne, Switzerland

The authors declare no competing financial interests.

## ACKNOWLEDGMENT

This work was supported by the European Research Council Advanced Grant STRATUS (ERC-2011-AdG No. 291198) to GC and MG. RBV is thankful for support from the European Commission through the Marie Curie actions (FP7-PEOPLE-IEF-2012). SM gratefully acknowledges the support of NSF, grant CHE 1663822.

## REFERENCES

- (1) Feringa, B. L.; Browne, W. R. *Molecular Switches 2<sup>nd</sup> Edition*; Wiley-VCH Verlag GmbH & Co. KgaA, **2011**.
- (2) Ikeda, T.; Tsutsumi, O. Optical Switching and Image Storage by Means of Azobenzene Liquid-crystal Films. *Science* **1995**, 268, 1873-1875.
- (3) Renner, C.; Moroder, L. Azobenzene as Conformational Switch in Model Peptides. *ChemBioChem* **2006**, 7, 868-878.

- (4) Spörlein, S.; Carstens, H.; Satzger, H.; Renner, C.; Behrendt, R.; Moroder, L.; Tavan, P.; Zinth, W.; Wachtveitl, J. Ultrafast Spectroscopy Reveals Subnanosecond Peptide Conformational Dynamics and Validates Molecular Dynamics Simulation. *Proc. Nat. Acad. Sci.* **2002**, *99*, 7998-8002.
- (5) Banghart, M. R.; Volgraf, M.; Trauner, D. Engineering Light-Gated Ion Channels. *Biochemistry* **2006**, *45*, 15129-15141.
- (6) Mahimwalla, Z.; Yager, K. G.; Mamiya, J.; Shishido, A.; Priimagi, A. Barrett, C. J. Azobenzene Photomechanics: Prospects and Potential Applications. *Polymer Bulletin* **2012**, *69*, 967-1006.
- (7) Munkerup, K.; Romanov, D.; Bohinski, T.; Stephansen, A.B; Levis, R. J.; Sølling, T. I. Conserving Coherence and Storing Energy during Internal Conversion: Photoinduced Dynamics of cis-and trans-Azobenzene Radical Cations. *The Journal of Physical Chemistry A* **2017**, *121*, 8642-8651.
- (8) Rau. H.; Lueddecke, E. On the Rotation-Inversion Controversy on Photoisomerization of Azobenzenes. Experimental Proof of Inversion. *J. Am. Chem. Soc.* **1982**, *104*, 1616-1620.
- (9) Rau., H. Photoisomerization of benzenes. In *Photoreactive Organic Thin Films*; Academic Press: Boston, **2002**.
- (10) Cho, J.; Berbil Bautista, L.; Levy, N.; Poulsen, D.; Fréchet, J. M. J.; Crommie, M. F. Functionalization, Self-assembly, and Photoswitching Quenching for Azobenzene Derivatives Adsorbed on Au (111). *J. Phys. Chem. C* **2010**, *133*, 234707.

- (11) Pechenezhskiy, I. V.; Cho, J.; Nguyen, G. D.; Berbil-Bautista, L.; Giles, B. L.; Poulsen, D. A.; Fréchet, J. M. J.; Crommie, M. F. Self-Assembly and Photomechanical Switching of an Azobenzene Derivative on GaAs (110): A Scanning Tunneling Microscopy Study. *J. Phys. Chem. C* **2012**, *116*, 1052–1055.
- (12) Bandara, H. M. D.; Burdette, S. C. Photoisomerization in Different Classes of Azobenzene. *Chem. Soc. Rev.* **2012**, *41*, 1809-1825.
- (13) Lednev, I. K.; Ye, T.; Hester, R. E.; Moore, J. N. Femtosecond Time-Resolved UV–Visible Absorption Spectroscopy of trans-Azobenzene in Solution. *J. Phys. Chem.* **1996**, *100*, 13338-13341.
- (14) Lednev, I. K.; Ye, T.; Matousek, P.; Towrie, M.; Foggi, P.; Neuwahl, F. V. R.; Umpathy, S.; Hester, R. E.; Moore, J. N. Femtosecond Time-Resolved UV-Visible Absorption Spectroscopy of trans-Azobenzene: Dependence on Excitation Wavelength. *Chem. Phys. Lett.* **1998**, *290*, 68-74.
- (15) Fujino J.; Tahara, T. Picosecond Time-Resolved Raman Study of trans-Azobenzene *J. Phys. Chem. A* **2000**, *104*, 4203-4210.
- (16) Fujino, T.; Arzhantsev, S. Yu.; Tahara, T. Femtosecond Time-Resolved Fluorescence Study of Photoisomerization of trans-Azobenzene. *J. Phys. Chem. A* **2001**, *105*, 8123-8129.
- (17) Fujino, T.; Arzhantsev, S. Yu.; Tahara, T. Femtosecond/Picosecond Time-Resolved Spectroscopy of trans- Azobenzene: Isomerization Mechanism Following  $S_2(\pi\pi^*)\leftarrow S_0$  Photoexcitation. *Bull. Chem. Soc. Jpn.* **2002**, *75*, 1031-1040.

- (18) Satzger, H.; Root, C.; Braun M. Excited-State Dynamics of trans- and cis-Azobenzene after UV Excitation in the  $\pi\pi^*$  Bband. *J. Phys. Chem. A* **2004**, *108*, 6265-6271.
- (19) Naegele, T.; Hoche, R.; Zinth, W.; Wachtveitl, J. Femtosecond Photoisomerization of cis-Azobenzene. *Chem. Phys. Lett.* **1997**, *272*, 489-495.
- (20) Satzger, H.; Spoerlein, S.; Root, C.; Wachtveitl, J.; Zinth, W.; Gilch, P. Fluorescence Spectra of trans- and cis-Azobenzene—Emission from the Franck–Condon State. *Chem. Phys. Lett.* **2003**, *372*, 216-223.
- (21) Schultz, T.; Quenneville, J.; Levine, B.; Toniolo, A.; Martinez, T. J.; Lochbrunner, S.; Schmitt, M.; Schaffer, J. P.; Zgierski, M. Z.; Stolow, A. Mechanism and Dynamics of Azobenzene Photoisomerization. *J. Am. Chem. Soc.* **2003**, *125*, 8098-8099.
- (22) Rau, H. Further Evidence for Rotation in the  $\pi,\pi^*$  and Inversion in the  $n,\pi^*$  Photoisomerization of Azobenzenes. *J. Photochem.* **1984**, *26*, 221-225.
- (23) Stuart, C. M.; Frontiera, R. R.; Mathies, R. A. Excited-State Structure and Dynamics of cis- and trans-Azobenzene from Resonance Raman Intensity Analysis. *J. Phys. Chem. A* **2007**, *111*, 12072-12080.
- (24) Kim, Y.; Philips, J. A.; Liu, H.; Kang, H.; Weihong, T. Using Photons to Manipulate Enzyme Inhibition by an Azobenzene-Modified Nucleic Acid Probe *Proc. Nat. Acad. Sci.* **2009**, *106*, 6489-6494.

- (25) Quick, M.; Dobrykov, A. L.; Gerecke, M.; Richter, C.; Berndt, F.; Ioffe, I. N.; Granovsky, A. A.; Mahrwald, R.; Ernsting, N. P.; Kovalenko, S. A. Photoisomerization Dynamics and Pathways of trans- and cis-Azobenzene in Solution from Broadband Femtosecond Spectroscopies and Calculations. *J. Phys. Chem. B* **2014**, *118*, 8756-8771.
- (26) Monti, S.; Orlandi, G.; Palmieri, P. Features of the Photochemically Active State Surfaces of Azobenzene. *Chem. Phys.* **1982**, *81*, 87-99.
- (27) Ishikawa, I.; Noro, T.; Shoda, T. Ishikawa T., Noro T. & Shoda T. Theoretical Study on the Photoisomerization of Azobenzene. *J. Chem. Phys.* **2001**, *115*, 7503-7512.
- (28) Conti, I.; Garavelli, M.; Orlandi, G. The Different Photoisomerization Efficiency of Azobenzene in the Lowest  $n\pi^*$  and  $\pi\pi^*$  Singlets: the Role of a Phantom State. *J. Am. Chem. Soc.* **2008**, *130*, 5216-5230.
- (29) Casellas, J.; Bearpark, M. J.; Reguero, M. Excited-State Decay in the Photoisomerisation of Azobenzene: A New Balance between Mechanisms. *ChemPhysChem* **2016**, *17*, 3068-3079.
- (30) Harabuchi, Y.; Ishii, M.; Nakayama, A.; Noro, T.; Taketsugu, T. A Multireference Perturbation Study of the NN Stretching Frequency of trans-Azobenzene in  $n\pi^*$  Excitation and an Implication for the Photoisomerization Mechanism. *J. Chem. Phys.* **2013**, *138*, 064305.
- (31) Tan, E. M. M.; Amirjalayer, S.; Smolarek, S.; Vdovin, A.; Zerbetto, F.; Buma, W. J. Fast Photodynamics of Azobenzene Probed by Scanning Excited-State Potential Energy Surfaces Using Slow Spectroscopy. *Nat. Commun.* **2015**, *6*, 5860.

- (32) Ootani, Y.; Satoh, K.; Nakayama, A.; Noro, T.; Taketsugu, T. Ab Initio Molecular Dynamics Simulation of Photoisomerization in Azobenzene in the  $n\pi^*$  State. *J. Chem Phys.* **2009**, *131*, 194306.
- (33) Yuan, S.; Dou, Y.; Wu, W.; Hu, Y.; Zhao, J. Why Does trans-Azobenzene Have a Smaller Isomerization Yield for  $\pi\pi^*$  Excitation than for  $n\pi^*$  Excitation? *J. Chem. Phys.* **2008**, *112*, 13326-13334.
- (34) Giustiano, T.; Muccioli, L.; Berardi, R.; Zannoni, C. How Does the trans-cis Photoisomerization of Azobenzene Take Place in Organic Solvents? *Chem. Phys. Chem.* **2010**, *11*, 1018-1028.
- (35) Cembran, A.; Bernardi, F.; Garavelli, M.; Gagliardi, L.; Orlandi, G. On the Mechanism of the cis-trans Isomerization in the Lowest Electronic States of Azobenzene:  $S_0$ ,  $S_1$ , and  $T_1$ . *J. Am. Chem. Soc.* **2004**, *126*, 3234-3243.
- (36) Altoe, P.; Bernardi, F.; Conti, I.; Garavelli, M.; Negri, F.; Orlandi, G. Light Driven Molecular Switches: Exploring and Tuning Their Photophysical and Photochemical Properties. *Theor. Chem. Acc.* **2007**, *117*, 1041-1059.
- (37) Conti, I.; Marchioni, F.; Credi, A.; Orlandi, G.; Rosini, G.; Garavelli, M. Cyclohexenylphenyldiazene: a Simple Surrogate of the Azobenzene Photochromic Unit. *J. Am. Chem. Soc.* **2007**, *129*, 3198-3210.
- (38) Böckmann, M.; Doltsinis, N. L.; Marx, D. Unraveling a Chemically Enhanced Photoswitch: Bridged Azobenzene. *Ang. Chem. Int. Ed.*, **2010**, *49*, 3382-3384.

- (39) Moreno, M.; Gelabert, R.; Lluch, J. M. The Quest for Photoswitches Activated by Near-Infrared Light. A Theoretical Study of the Photochemistry of BF<sub>2</sub>-Coordinated Azo Derivatives. *ChemPhysChem* **2016**, *17*, 2824-2838.
- (40) Borrego-Varillas, R.; Candeo, A.; Viola, D.; Garavelli, M.; De Silvestri, S.; Cerullo, G.; Manzoni, C. Microjoule-Level, Tunable Sub-10 fs UV Pulses by Broadband Sum-Frequency Generation. *Opt. Lett.* **2014**, *39*, 3849-3852.
- (41) Borrego-Varillas, R.; Oriana, A.; Branchi, F.; De Silvestri, S.; Cerullo, G.; Manzoni, C. Optimized Ancillae Generation for Ultra-Broadband Two-Dimensional Spectral-Shearing Interferometry. *J. Opt. Soc. Am. B*, **2015**, *32*, 1851-1855.
- (42) Borrego-Varillas, R.; Oriana, A.; Ganzer, L.; Trifonov, A.; Buchvarov, I.; Manzoni, C.; Cerullo, G. Two-Dimensional Electronic Spectroscopy in the Ultraviolet by a Birefringent Delay Line. *Opt. Express*, **2016**, *24*, 28491-28499.
- (43) Mukamel, S. Principles of Nonlinear Optical Spectroscopy; Oxford University Press: New York, **1995**.
- (44) Mukamel, S.; Abramavicius, D. Many-Body Approaches for Simulating Coherent Nonlinear Spectroscopies of Electronic and Vibrational Excitons. *Chem. Rev.* **2004**, *104*, 2073-2098.
- (45) Abramavicius, D.; Palmieri, B.; Voronine, D. V.; Sanda, F.; Mukamel, S. Coherent Multidimensional Optical Spectroscopy of Excitons in Molecular Aggregates; Quasiparticle versus Supermolecule Perspectives. *Chem. Rev.* **2009**, *109*, 2350-2408.

- (46) Nenov, A.; Rivalta, I.; Mukamel, S.; Garavelli, M. Bidimensional Electronic Spectroscopy on Indole in Gas Phase and in Water from First Principles. *Comput. Theor. Chem.* **2014**, *1040-1041*, 295-303.
- (47) Nenov, A.; Mukamel, S.; Garavelli, M.; Rivalta, I. Two-Dimensional Electronic Spectroscopy of Benzene, Phenol, and Their Dimer: an Efficient First-Principles Simulation Protocol. *J. Chem. Theory Comput.* **2015**, *11*, 3755-3771.
- (48) Nenov, A.; Giussani, A.; Segarra-Martí, J.; Jaiswal, V. K.; Rivalta, I.; Cerullo, G.; Mukamel, S.; Garavelli, M. Modeling the High-Energy Electronic State Manifold of Adenine: Calibration for Nonlinear Electronic Spectroscopy. *J. Chem. Phys.* **2015**, *142*, 212443.
- (49) van Stokkum, I. H. M.; Larsen, D. S.; van Grondelle, R. Global and Target Analysis of Time-Resolved Spectra. *Biochim. Biophys. Acta* **2004**, *1657*, 82-104.
- (50) Snellenburg, J. J.; Liptonok, S. P.; Seger, R.; Mullen, K. M.; van Stokkum, I. H. M. Glotaran: A Java-Based Graphical User Interface for the R Package TIMP. *J. Stat. Software* **2012**, *49*, 1-22.
- (51) Pepino, A. J.; Segarra-Martí, J.; Nenov, A.; Improta, R.; Garavelli, M. Resolving Ultrafast Photoinduced Deactivations in Water-Solvated Pyrimidine Nucleosides. *J. Phys. Chem. Lett.* **2017**, *8*, 1777-1783.